Simulation of Brillouin gain properties in a double-clad As_2Se_3 chalcogenide photonic crystal fiber

Xin Chen (陈 欣), Li Xia (夏 历), Wei Li (李 微)*, and Chen Li (李 晨)

School of Optical and Electronic Information, Huazhong University of Science and Technology, Wuhan 430074, China
**Corresponding author: weili@hust.edu.cn*

Received October 12, 2016; accepted December 28, 2016; posted online February 2, 2017

The Brillouin gain properties in a double-clad As_2Se_3 photonic crystal fiber (PCF) are simulated based on the finite-element method (FEM). The results indicate that the Brillouin gain spectrum (BGS) of our proposed chalcogenide PCF exhibits a multipeaked behavior and has a high Brillouin gain coefficient. We also find that a larger size of inner cladding air holes will lead to a more pronounced second peak in the BGS. On the other hand, the size of the outer cladding has nearly no effect on the BGS behavior. Through these results, one can tailor the Stimulated Brillouin scattering effect in PCFs for a wide range of applications.

OCIS codes: 290.5900, 190.4370, 060.4370, 060.5295.
doi: 10.3788/COL201715.042901.

Stimulated Brillouin scattering (SBS) in fibers is a nonlinear optical phenomenon caused by the interaction between optical and acoustic waves propagating in the medium, and it plays an important role in optical systems. This nonlinear effect, due to its lower threshold and other intrinsic properties, has already been extensively studied. Nowadays there are many applications exploiting the SBS effect, like slow light generation[1], fiber optics sensors[2], fiber amplifiers[3], fiber lasers[4], and microwave signal processing[5]. For those applications, it is quite necessary to enhance the SBS in fibers. However, in other applications like high-power fiber lasers[6,7], high-power fiber amplifiers[6–10], and telecommunication systems, SBS effect is harmful and should be suppressed. In fact, many researchers have been focusing on enhancing or mitigating the SBS effect in fibers so as to tailor the Brillouin response for a particular application[6–13].

Photonic crystal fibers (PCFs) with unique and remarkable Brillouin scattering properties as well as a novel and flexible structure have already been widely investigated. One can either suppress or enhance the SBS effect in PCFs by designing a certain PCF structure. In spite of the promising results researchers have achieved on many kinds of PCFs[14,15], a systematic investigation of SBS properties in double-clad PCFs that are made up of highly nonlinear material is still lacking.

In this Letter, we present a full-modal analysis of optical and acoustic modes in a double-clad As_2Se_3 PCF, and numerically study its Brillouin gain (BG) properties. We also investigate the influence of structure parameters on the Brillouin gain spectrum (BGS) properties, thus we can tailor the SBS effect for a wide range of applications like a distributed Brillouin fiber sensor. The simulation process is accomplished by a commercial finite element method (FEM) solver—COMSOL Multiphysics.

In PCFs, SBS can result from the interaction between optical modes and multiple acoustic modes like shear modes, longitudinal modes, or even surface modes[16]. These acoustic modes, which travel at different phase velocities, have different contributions to the BGS. Among them, longitudinal modes are the most dominant component, thus in this Letter we only consider their influence on BGS. Many theoretical researchers have indicated that we can calculate the BGS through solving the optical and acoustic wave equations[11,17].

The 2D scalar-wave equation governing the acoustic displacement distribution $u(x, y)$ can be expressed as[17]

$$\nabla_t^2 u + \left(\frac{\omega_a^2}{v_l^2} - \beta_a^2\right) u = 0, \tag{1}$$

where ω_a is the angular frequency of the acoustic wave, ν_l is the longitudinal acoustic velocity in PCFs, and β_a is the acoustic propagation constant. ν_l varies on the cross section of PCFs according to the material, doping type, and doping concentration as well as the temperature and strain displacement. The backscattered SBS only happens when $\beta_a = 2\beta_p$, where $\beta_p = 2\pi n_{\text{eff}}/\lambda_p$ is the optical propagation constant, n_{eff} is the effective index of optical fundamental mode, and λ_p is the pump wavelength.

The Brillouin frequency shift (BFS) of the ith-order longitudinal acoustic mode can be expressed as

$$f_{B,i} = \frac{\omega_{a,i}}{2\pi}. \tag{2}$$

The contribution of the ith-order longitudinal acoustic mode to the BGS is determined by the overlap between the acoustic modes and the optical fundamental mode, and can be expressed as[17]

$$S_{B,i}(f) = \frac{(\Delta f_B/2)^2}{(\Delta f_B/2)^2 + (f - f_{B,i})^2}\, g_{B,i} I_i, \tag{3}$$

where I_i is the overlap integral between the optical and the ith-order acoustic modes, Δf_B is the full width at half-maximum (FWHM) of the BGS and is related to

the phonon lifetime in the material. In order to simplify the calculation, we assume that all the acoustic modes share the same FWHM value. We can see from Eq. (3) that the BG reaches a maximum when $f = f_{B,i}$, and the maximum BG equals $I_i g_{B,i}$. I_i is given by[11]

$$I_i = \frac{\left(\iint |E|^2 u_i^* \mathrm{d}x\mathrm{d}y\right)^2}{\iint |E|^4 \mathrm{d}x\mathrm{d}y \iint |u_i|^2 \mathrm{d}x\mathrm{d}y}, \tag{4}$$

where $E(x, y)$ is the field pattern of the optical fundamental mode. The integral is calculated on the cross section of the PCFs.

$g_{B,i}$ is given by[11]

$$g_{B,i} = \frac{4\pi n_{\mathrm{eff}}^8 p_{12}^2}{\lambda_p^3 \rho c f_{B,i} \Delta f_B}, \tag{5}$$

where p_{12} is longitudinal photoelastic coefficient and ρ is the material density.

Since all the acoustic modes are statistically independent, the total BGS of PCFs can be expressed as[11]

$$S_B(f) = \sum_i S_{B,i}(f). \tag{6}$$

The simulation process is accomplished using COMSOL. Since the SBS effect results from the interaction between optical and acoustic waves, we need to use the multiphysics field when computing the BGS properties. We choose the radio frequency (RF) module to calculate the optical modes, the coefficient form partial differential equation (PDE) module to obtain acoustic modes. In the RF module, we set the exterior boundaries' condition to be a perfect electric conductor (PEC). In the PDE module, the boundary condition of the exterior boundaries is the Dirichlet boundary (which means there is no field outside the PCF), and the boundary condition of interior boundaries is the Neumann boundary. To balance the accuracy and efficiency of the simulation process, we set the mesh type to be free triangular and the mesh size to be finer.

When simulating, we first use the RF module to calculate optical parameters $E(x, y)$ and n_{eff}, then we can calculate all the longitudinal acoustic field distributions $u_i(x, y)$ and its corresponding ω_a by introducing the value of β_a into the PDE module. Finally, we can calculate the overlap integral between the optical fundamental mode and the ith-order acoustic modes by Eq. (4), thus the BGS of our proposed PCF can be easily deduced.

Here, we investigate the BGS properties of a double-clad As_2Se_3 chalcogenide PCF. The schematic illustration of our proposed PCF is shown in Fig. 1(a). This PCF has four hexagonal rings: the inner two rings form the inner cladding, air hole diameter $d_1 = 0.8$ μm; while the other two rings form the outer cladding, air hole diameter $d_2 = 1.2$ μm. The hole-to-hole pitch is $\Lambda = 2$ μm. For As_2Se_3 glass, the refractive index is $n_{\mathrm{eff}} = 2.808$, the material density is $\rho = 4640$ kg/m^3, the acoustic velocity $\nu_l = 2250$ m/s, the longitudinal photoelastic coefficient and the FWHM are, respectively, $p_{12} = 0.266$ and $\Delta f_B = 13.2$ MHz.

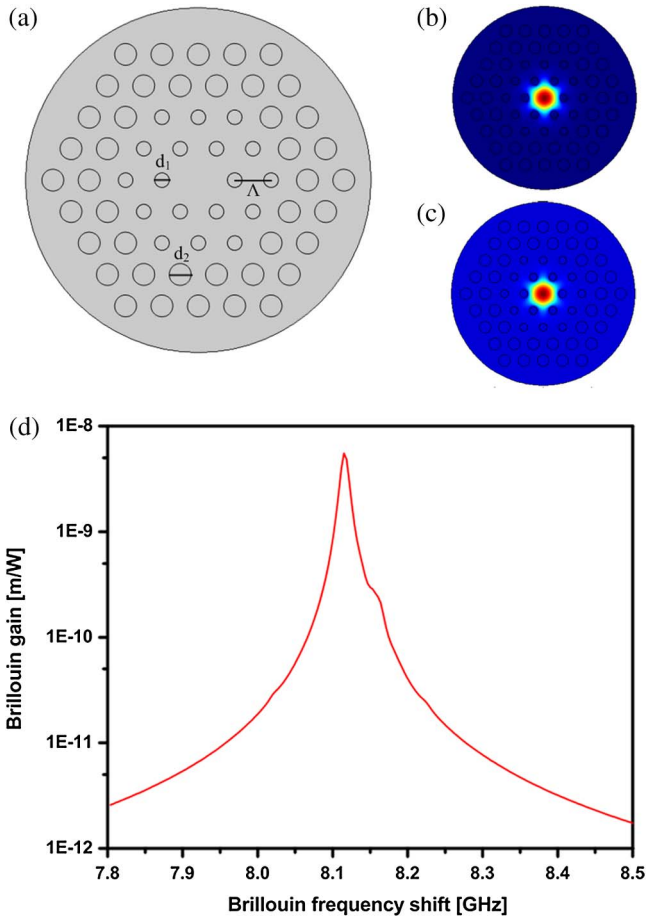

Fig. 1. (a) Schematic illustration of the double-clad As_2Se_3 PCF, (b) the electric field distribution of the fundamental optical mode, (c) the acoustic displacement distribution of the fundamental acoustic mode, and (d) the BGS of the As_2Se_3 PCF structure with $d_1 = 0.8$ μm, $d_2 = 1.2$ μm, and $\Lambda = 2$ μm.

Figures 1(b) and 1(c) show the field distribution of the optical and acoustic fundamental modes. The BGS of this As_2Se_3 PCF that we calculated is shown in Fig. 1(d). We can see that there are two peaks in the BGS. For the main peak, which corresponds to the acoustic fundamental mode, the BFS = 8.115 GHz and the corresponding BG reaches 5.51×10^{-9} m/W, which is about 320 times larger than that of silica PCFs[17].

We now investigate the influence of structure parameters on SBS properties in our double-clad As_2Se_3 PCF. Figure 2(a) depicts the BGSs of three different PCF structures when increasing d_1 ($d_1 = 0.8$, 1.2, and 1.6 μm).We can see that the BGS exhibits a multipeaked behavior and the second peak becomes more pronounced when d_1 increases. This is because, when d_1 increases, the effective mode area begins to decrease, and the PCF confinement ability of both the optical and acoustic modes increase. Thus, the Brillouin threshold is reduced, the SBS effect is enhanced, and more high-order acoustic modes are confined in the core. From Eqs. (3)–(5), we can infer that the value of the BG strongly depends on the overlap between the optical and acoustic modes. Therefore, the increase of

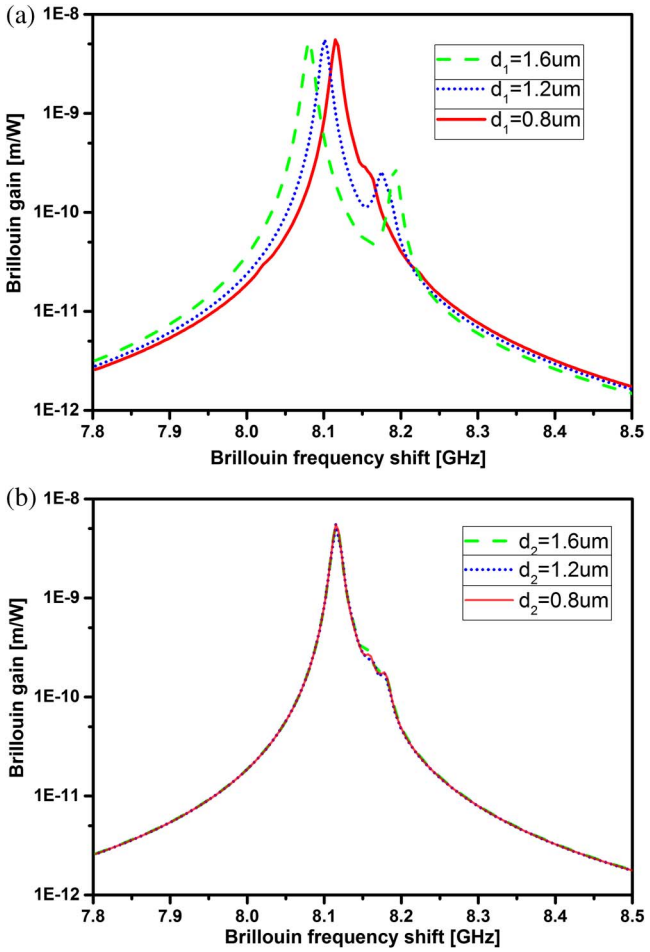

Fig. 2. BGS of three double-clad As_2Se_3 PCF structures with (a) $d_2 = 1.2$ μm, $\Lambda = 2$ μm and $d_1 = 0.8$, 1.2, and 1.6 μm; (b) $d_1 = 0.8$ μm, $\Lambda = 2$ μm, and $d_2 = 0.8$, 1.2, and 1.6 μm.

the inner-clad diameter can result in a more pronounced second peak. In addition, we note that when d_1 increases, the BFS of the main peak decreases and the BFS of the second peak increases. When $d_1 = 0.8$, 1.2, and 1.6 μm, the corresponding BFSs of the main peak are, respectively, 8.115, 8.101, and 8.080 GHz, and the corresponding BFSs of the second peak are, respectively, 8.154, 8.175, and 8.192 GHz. This phenomenon is due to the strong index contrast between the core and the inner cladding.

Figure 2(b) depicts the BGSs of different PCF structures when increasing the outer cladding air hole diameter d_2 ($d_2 = 0.8$, 1.2, and 1.6 μm). We can see from this picture that when d_2 increases, the BGS of our proposed PCF remains almost the same. All these three curves exhibit a multipeaked structure, and the very weak second peaks stay close to the main peaks. The BFSs of the main peaks and the second peaks are fixed, respectively, at 8.115 and 8.154 GHz. This is because when d_2 changes, the optical fundamental mode, the effective index, and the effective mode area remain the same, so the acoustic propagation constant stays unchanged and the overlap between the optical fundamental mode and acoustic modes confined in the core is substantially retained.

In this Letter, we present the numerical results of the BGS properties in double-clad As_2Se_3 PCF based on the FEM. Our obtained results indicate that the proposed PCF exhibits a multipeaked behavior and owns a high BG coefficient. When the inner cladding air-hole diameter d_1 increases, the SBS effect in PCF is strongly enhanced, the BGS exhibits a more pronounced second peak, and the main peak has a left shift while the second peak begins to move right. However, the change of the outer cladding air hole diameter d_2 will not affect the BGS behavior of our proposed PCF.

This work was supported by the International Cooperation Projects between China and Singapore under Grant No. 2009DFA12640.

References

1. M. G. Herráez, K. Song, and L. Thévenaz, Opt. Express **14**, 1395 (2006).
2. X. Bao, Opt. Photon. News **20**(9), 40 (2009).
3. Z. Lu, W. Gao, W. He, Z. Zhang, and W. Hasi, Opt. Express **17**, 10675 (2009).
4. Z. Liu, Y. Wang, Y. Wang, H. Yuan, Z. Bai, H. Wang, R. Liu, S. Li, H. Zhang, L. Zhou, T. Tan, W. He, and Z. Lu, Chin. Opt. Lett. **14**, 091901 (2016).
5. R. Pant, D. Marpaung, I. Kabakova, B. Morrison, C. G. Poulton, and B. J. Eggleton, Laser Photon. Rev. **8**, 653 (2014).
6. M. D. Mermelstein, M. J. Andrejco, J. Fini, C. Headley, and D. J. DiGiovanni, Proc. SPIE **7580**, 75801G (2010).
7. R. Engelbrecht, J. Hagen, and M. Schmidt, Proc. SPIE **5777**, 795 (2005).
8. L. Zhang, S. Cui, J. Hu, J. Wang, C. Liu, J. Zhou, and Y. Feng, in *Conference on Lasers and Electro-Optics (CLEO)* (2013), paper CF1E.7.
9. V. I. Kovalev and R. G. Harrison, Opt. Lett. **31**, 161 (2006).
10. J. E. Rothenberg, P. A. Thielen, M. Wickham, and C. P. Asman, Proc. SPIE **6873**, 68730O (2008).
11. T. Cheng, M. Liao, W. Gao, Z. Duan, T. Suzuki, and Y. Ohishi, Opt. Express **20**, 28846 (2012).
12. M. Lorenzen, D. Noordegraaf, C. Nielsen, O. Odgaard, L. Gruner-Nielsen, and K. Rottwitt, Electron. Lett. **45**, 125 (2009).
13. M. Hu, Z. Quan, J. Wang, K. Liu, X. Chen, C. Zhao, Y. Qi, B. He, and J. Zhou, Chin. Opt. Lett. **14**, 031403 (2016).
14. P. Dainese, N. Joly, E. Davies, J. Knight, P. Russell, and H. Fragnito, in *Conference on Lasers and Electro-Optics/International Quantum Electronics Conference and Photonic Applications Systems Technologies* (2004), paper CThHH3.
15. L. Zou, X. Bao, and L. Chen, Opt. Lett. **28**, 2022 (2003).
16. J. Beugnot, S. Lebrun, G. Pauliat, H. Maillotte, V. Laude, and T. Sylvestre, Nat. Commun. **5**, 5242 (2014).
17. R. Cherif, M. Zghal, and L. Tartara, Opt. Commun. **285**, 341 (2012).